UC-25+37
LBL-17483 c.1

Lawrence Berkeley Laboratory
UNIVERSITY OF CALIFORNIA

Engineering & Technical Services Division

Presented at the Third International Conference on Infrared Physics, Zurich, Switzerland, July 23-27, 1984; and submitted to Infrared Physics

PHYSICS AND DESIGN OF ADVANCED INFRARED BOLOMETERS AND PHOTOCONDUCTORS

E.E. Haller

July 1984

RECEIVED
LAWRENCE
BERKELEY LABORATORY
SEP 10 1984
LIBRARY AND
DOCUMENTS SECTION

For Reference
Not to be taken from this room

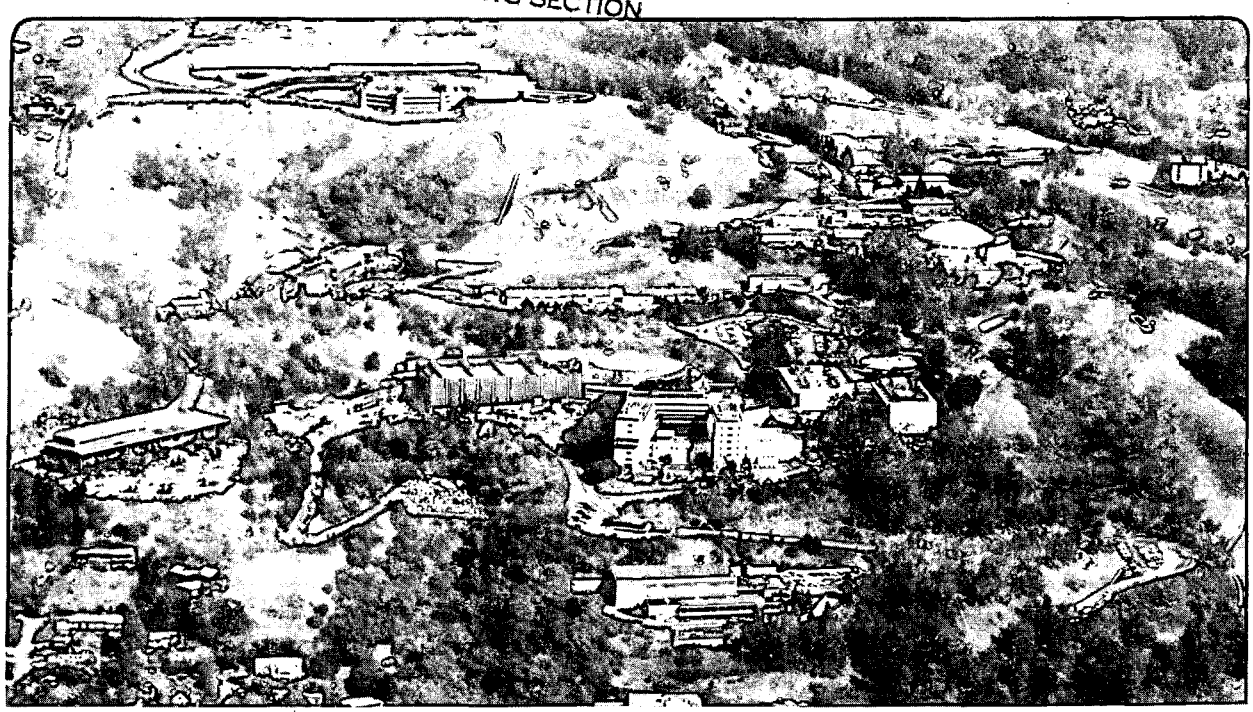

Prepared for the U.S. Department of Energy under Contract DE-AC03-76SF00098

LBL-17483 c.1

DISCLAIMER

This document was prepared as an account of work sponsored by the United States Government. While this document is believed to contain correct information, neither the United States Government nor any agency thereof, nor the Regents of the University of California, nor any of their employees, makes any warranty, express or implied, or assumes any legal responsibility for the accuracy, completeness, or usefulness of any information, apparatus, product, or process disclosed, or represents that its use would not infringe privately owned rights. Reference herein to any specific commercial product, process, or service by its trade name, trademark, manufacturer, or otherwise, does not necessarily constitute or imply its endorsement, recommendation, or favoring by the United States Government or any agency thereof, or the Regents of the University of California. The views and opinions of authors expressed herein do not necessarily state or reflect those of the United States Government or any agency thereof or the Regents of the University of California.

Eugene E. Haller

PHYSICS AND DESIGN OF ADVANCED INFRARED BOLOMETERS AND PHOTOCONDUCTORS

Department of Materials Science and Lawrence Berkeley Laboratory, University of California, Berkeley, CA 94720 U.S.A.

ABSTRACT

Spaceborn infrared telescopes and other very low photon flux experiments require photoconductors and bolometers with ever increasing sensitivity working at the background limit. Improvements in the understanding of the physics of these devices, advances in semiconductor materials synthesis and device technology, and the introduction of new device concepts such as uniaxially stressed photoconductors can, in combination, fulfill these new demands.

1. INTRODUCTION

The typical infrared photon detection situation is characterized by two distinct photon streams impinging on a detector: background photons (background photon power P_B) and signal photons (signal photon power P_S). The fluctuations in the photon streams produce fluctuations in the detector signal. It is this noise which sets an absolute lower limit for the detection of signal photons. We define an "ideal" detector as one in which the noise produced by effects in the detector unrelated to photons and the electronic circuits used to amplify the signal is negligibly small compared with the photon noise. A device which works as an "ideal" detector for observations in ambient temperature on the earth may be completely inadequate (i.e., far from ideal) in an ultra-low background environment such as, for example, outer space. Scientists were faced with precisely this situation during the development of the first dedicated Far Infrared Astronomical Satellite (IRAS) [1]. Low background flux experiments are, however, not limited to outer space. Narrow band experiments and experiments in an appropriately cooled environment may also be characterized by a low photon background flux.

The strong interest in "ideal" detectors operating in very low backgrounds marked the beginning of an era of rapid development of novel and improved detectors and detector systems (one- and two-dimensional arrays) working over a broad infrared spectrum ranging from $\lambda \sim 3$ μm to 1000 μm. We find ourselves today in the midst of a detector evolution and it is the goal of this summary to point out some of the most important and interesting developments. Partly due to personal interest and involvement and partly due to their importance, we will discuss uniaxially stressed extrinsic photoconductors, multi-impurity level effects in extrinsic photoconductors, and neutron transmutation doping (NTD) of germanium for bolometer fabrication in some detail. These discussions will also illustrate the symbiotic

relationship between infrared physics and characterization of semiconductors and the development of infrared detection devices.

2. EXTRINSIC SEMICONDUCTOR PHOTOCONDUCTORS

2.1 Basic Detector Physics and Figures of Merit

An excellent review of photoconductors made from extrinsic semiconductors has been given by Bratt [2]. For the following discussion, we assume that the photoconductor crystal contains N_D majority shallow donor impurities and N_A minority shallow acceptor impurities, (i.e., $N_D > N_A$). At very low temperatures ($kT << E_D$, E_D = binding energy of the electrons to the donors) and in the dark, $(N_D - N_A)$ donors will bind an electron and are therefore neutral while N_A donors will have given up their electron to the compensating acceptors. The number of electrons in the conduction band will be extremely small, resulting in high resistivity. When photons with $h\nu \geq E_D$ enter the crystal and are absorbed by neutral donors, bound electrons will be excited into the conduction band. The free electrons will travel in the externally applied electric field E with a velocity v:

$$v = \mu E \tag{1}$$

The electron drift corresponds to an electric current. At the typical low free carrier concentrations, a photoconductor detector (Fig. 1) can be modeled with a capacitor filled with a dielectric. The capacitor electrodes are the contacts. The interelectrode distance shall be L. The average distance l traveled by the photogenerated electron in the average lifetime τ is:

$$l = v\tau = \mu E\tau \tag{2}$$

The ratio of the mean free electron path l to the interelectrode distance L is called photoconductive gain G. (Note that G can be larger than one.) If $\dot{N}$ photons per second enter the crystal and a fraction η, called quantum efficiency, (η has a value between 0 and 1) of these photons leads to donor ionization, a signal current

$$I_S = e\dot{N}\eta\ l/L = e\dot{N}\eta\ \mu E\tau/L = e\dot{N}\eta G \tag{3}$$

flows in the external detector circuit.

The quantities η and G are important figures of merit for a detector. With the proper choice of optics, detector geometry, doping concentration, and detector cavity design, η approaches 1. Values of $\eta \lesssim 0.01$ are, however, frequently encountered in non-optimized systems. The value of G can vary over a broad range. Photoconductors made from doped germanium and silicon exhibit values of G of up to 10 but values of G between 0.1 and 1 are more typical. The concentration of ionized donors controls the lifetime τ. Because this concentration is equal* to the number of minority acceptors, it is important to reduce the acceptor concentration to low values in order to obtain

*The concentration of ionized donors can become larger than the acceptor concentration under very strong illumination. This is a regime which we do not consider here.

high photoconductive gain. This point needs further refinement because the maximum field which can be applied can also depend on the minority impurity concentration. A third figure of merit is the responsivity R which is directly proportional to the $G\eta$ product:

$$R = I_S/P_S = G\eta e/h\nu \tag{4}$$

where P_S = incident signal photon power = $\dot{N}_S h\nu$. The responsivity is measured in A/W. Values of R reach up to 100 A/W for the very best silicon photoconductors, while typical values range from 1 to 20 A/W. Large values of R are important and preferred because they imply large signals. A large signal is more easily amplified without the introduction of noise added by the first stage(s) of the amplifier.

2.2 Noise

Without a discussion of the noise produced in the detector by fluctuations in the photon stream and other detector related noise sources, one cannot define the ultimate sensitivity of a photoconductor. The noise equivalent power (NEP) is defined as the signal photon power required to produce a signal current I_S equal to the square root of the sum of the squares of all the noise currents, $\sqrt{\sum_i I_{n,i}^2}$, in an electrical bandwidth of Δf = 1 Hz:

$$NEP = \frac{\sqrt{\sum_i I_{n,i}^2 \Delta f}}{R} \tag{5}$$

In the ideal case, the noise is only produced by the photon-related fluctuations. This background limited infrared photoconductor noise equivalent power (NEP_{BLIP}) is:

$$NEP_{BLIP} = \sqrt{2(2\dot{N}_{total})(h\nu)^2} \tag{6}$$

where $\dot{N}_{total}$ = sum of the rates of background photons entering the detector. The first factor of 2 in Eq. 6 arises from the fact that both the generation of photo excited electrons and the recombination of these electrons are random, uncoupled processes. It is interesting to note that the factor 2 reduces to 1 in Eq. 6 for photodiodes. In photodiodes the charge carriers travel all the way to the contacts so that there exists no randomness in the recombination. The second factor of 2 is due to the shot noise associated with photocarrier generation.

Figure 2 shows a hypothetical performance curve of a photoconductor. The NEP above a background photon power P_{CRIT} increases proportionately to the square root of the power impinging on the detector, assuming Poisson's statistics. The detector may not reach the NEP_{BLIP} limit either because not all the photons are absorbed and create free carriers or because of excess noise. This less than ideal behavior can be expressed as an effective quantum efficiency, commonly called detective quantum efficiency $\eta_d \leq 1$:

$$\eta_d = \left(\frac{NEP_{BLIP}}{NEP}\right)^2 \tag{7}$$

Below P_{CRIT} the noise associated with the amplifier electronics dominates. It is in this regime where a reduction in amplifier noise and an increase in responsivity help extend the photon noise limited performance to lower photon power levels.

2.3 Advances in Photoconductor Materials

The inverse dependence of a photoconductor signal current on the interelectrode distance (Eq. 3) suggests that one should attempt to make the photoconductor as thin as possible. Since the linear optical absorption coefficient is proportional to the neutral majority dopant centers ($N_D - N_A$ at low temperatures), this means that high dopant concentrations are desirable. Hopping conduction—the tunneling of an electron from a neutral donor to a neighboring ionized donor—limits the maximum dopant concentration in silicon to ~ 10^{16} to 10^{17} cm^{-3} and in germanium to ~ 2 x 10^{14} cm^{-3} for shallow, hydrogenic impurities [3]. Above these concentrations carrier hopping increases the "dark" current (i.e., thermally generated current in the absence of a photon flux) unacceptably. Hopping also depends on the presence of ionized centers. As we have seen in the last section, these are mainly due to the minority impurities. This means that there are two arguments in favor of a low minority impurity concentration: a) increase in lifetime with decreasing minority impurity concentration, and b) decrease in hopping conduction. Until a few years ago the lowest residual impurity concentrations which could be achieved were of the order of 10^{12} cm^{-3} in germanium and 10^{13} cm^{-3} in silicon. The development of ultra-pure Ge and Si for use in nuclear radiation detectors [4] has lowered these limits by about two orders of magnitude. Using an ultra-pure germanium crystal growth facility, we have grown "purely" gallium-doped crystals for photoconductor use. The advantage of the low minority impurity concentration could not, however, be fully realized because these detectors show a lower breakdown field than conventional photoconductors [5]. The holes which are accelerated in the electric field suffer less scattering in the purer material and reach avalanche breakdown velocities at rather low fields ($E < 1$ Vcm^{-1}). The addition of neutral scattering centers—copper, a deep triple acceptor in the case of germanium—increases the breakdown field to the usual values while maintaining the advantages of the purely doped material. Results obtained with detectors made from such material will be discussed in another paper at this conference [6].

Silicon photoconductors have also undergone dramatic improvements. The floating zone technique [7] allows the growth of doped crystals with extremely low residual impurity concentrations. Responsivities of tens of A/W have been reported [8].

2.4 Contacts

The discussion of photoconductor physics and performance has so far not included the effects of contacts. The detailed understanding of contacts is quite limited. This is illustrated by the fact that no comprehensive physical model of photoconductors which includes the diffusion potential barriers at the contacts has been created. There exists an abundance of equivalent circuits which describe the behavior of detectors under pulsed light conditions and which try to account for a number of time constants which have been observed under certain circumstances. This equivalent circuit simulation has unfortunately not led to a better understanding of the physical mechanisms taking place inside a detector.

Despite the limited knowledge of the precise dependence of potential, electrical field, and space charge near the contacts, one can state that the transition from the metal contact wires to the bulk of the photoconductor should not be hindered by large potential barriers. A direct transition from a metal to a moderately-doped semiconductor is usually characterized by a high barrier (Schottky barrier) and is inadequate. A thin, heavily-doped layer between the metal and the photoconductor bulk strongly reduces the effective barrier. Carrier tunneling takes place between the metal and the heavily-doped region, and a relatively small diffusion barrier builds up between the heavily-doped region and the photoconductor bulk [9]. Impurity diffusion requiring high temperatures and long times has been replaced in recent years by ion implantation followed by a thermal annealing cycle. An implantation energy of 25 - 100 keV and a dose of 10^{14} - 10^{15} boron ions cm^{-2} for p-type Si or Ge and the same dose of phosphorus for n-type Si or Ge leads to p^{++} and n^{++} contacts respectively (++ indicates degenerately doped). Metallization after appropriate annealing with a few hundred Å of Pd followed by a few thousand Å of Au leads to low noise contacts with perfectly symmetrical photoconductor performance in regard to voltage bias polarity. Work towards a model which includes the photoconductor bulk as well as the contacts is in progress and should lead to a much better understanding of time dependent effects as a function of high bias and of energetic radiation.

2.5 Multilevel Semiconductors

In the previous chapters, the assumption was made that only one kind of majority and one kind of minority impurity were present in a photoconductor. Depending on the wavelength range of interest, one chooses impurities with appropriate electron or hole groundstate energies. For the 3 - 5 μm range, silicon doped with the acceptor indium (Si:In) offers an ideal choice [2]. The indium hole ground state lies at E_V + 156 meV (E_V = energy at the valence band top) leading to a photoconductive onset at $\lambda \sim 8$ μm. Every silicon crystal contains unavoidably some residual boron acceptors with a hole binding energy of E_V + 45 meV. A further level called InX which has been linked to an In-C center is located at E_V + 111 meV [10]. Besides these three acceptor levels, there are always phosphorus donor levels present. Alexander et al [8]* have evaluated the influence of the temperature and compensation of the shallow levels on detector responsivity. At very low temperature operation, when thermal generation from even the shallowest residual acceptor (E_{boron} = 45 meV) is negligible, highest responsivity is always obtained by minimizing the concentration of residual donors. For higher temperature operation, however, it is necessary to adjust the donor concentration to completely compensate all shallow residual acceptors to avoid contributions to the dark current. Very high responsivities may be obtained when the shallow acceptors are closely compensated because the effective cross section for capture in these centers is small due to the high probability of thermal re-emission, leading to long free carrier lifetimes. Values of 10^2 A/W have ben attained in Si:In. The close to perfect compensation has been achieved by a doping process using the transmutation of ^{30}Si nuclei into ^{31}P nuclei by thermal neutron capture followed by beta decay [11]. This Neutron Transmutation Doping (NTD)

*Figures 5 and 6 in Ref. 8 are exchanged by mistake.

has become very popular for the uniform doping of silicon used in the fabrication of high voltage, high power diodes and thyristors. We will come back to NTD when we discuss germanium bolometer material.

Another multilevel material which has been specifically developed for the λ = 30 - 50 μm range is beryllium-doped germanium (Ge:Be). Beryllium forms a double acceptor with hole binding energies at 24.5 meV and 58 meV [12]. The first beryllium level interacts via the photon generation of holes with the residual acceptor levels in a way similar to the Si:In system. The inherently lower doping concentrations in germanium required residual acceptor and donor concentrations as low as 10^{10} to 10^{11} cm^{-3}. Such low levels have only recently been achieved in nuclear radiation detector material. Using an ultra-pure crystal growth facility modified by removing the synthetic quartz crucible and the hydrogen atmosphere in order to prevent beryllium oxidation, we have obtained crystals which yield Ge:Be photoconductors with a responsivity of 10 A/W at λ = 42 μm and an NEP ≈ 1.7 x 10^{-16} $W/\sqrt{Hz}$ at a photon background flux of 7.1 x 10^{-13} W on the detector cavity aperture. The NEP_{BLIP} for an ideal detector would be 1.15 x 10^{-16} $W/\sqrt{Hz}$ which means that η_d ≈ 46%. This is the best result ever pulished at this wavelength [13].

2.6 Uniaxially Stressed Photoconductors

The shallowest impurity levels in germanium have binding energies close to 10 meV, corresponding to a photoconductive onset at about ν = 80 cm^{-1} (λ = 125 μm). Compound semiconductors such as GaAs exhibit lower donor binding energies which, in principle, should permit a longer wavelength onset. Such shallow donors have, however, very large electron orbits and the concentration of impurities has to be kept lower than in germanium if hopping conduction shall be avoided. At the present time it is not possible to grow III - V compound bulk semiconductor crystals which are pure enough and have sufficiently small defect concentrations to serve as photoconductor material for high performance, long wavelength detectors. A way to extend the sensitive range of gallim-doped germanium photoconductors to longer wavelength involves uniaxial stress. The change of the valence band structure under [100] stress (the light hole band pushes up through the heavy hole band) leads to an acceptor binding energy reduction by a factor of up to two [14]. This effect has been successfully utilized for Ge:Ga photoconductors [15] extending the sensitive range to ~ 240 μm (Fig. 3). Several groups have in the meantime successfully used this effective method. The same effects, though less pronounced, can be observed for acceptors in Si [16]. The small change in binding energy does not warrant the additional complications, especially now that high quality Ge:Be detectors which work very well in this wavelength range have become available [13].

3. SEMICONDUCTOR BOLOMETERS

3.1 Bolometer Physics and Figures of Merit

The physical principles governing photon detection with bolometers [17] are completely different from photoconductors. The change in conductivity due to a temperature change of a piece of material, in this case a semiconductor, is used to create a signal. One immediately obvious advantage is that bolometers work for any wavelength as long as the photons are absorbed. This may require special schemes such as composite bolometers consisting of an absorber coupled tightly to the sensing

element. Figure 4 shows the basic thermal circuit of a bolometer. The following equation describes the heat flow from the bolometer to the heat sink:

$$\eta P = H\left(\frac{d\Theta}{dt}\right) + G\Theta \tag{8}$$

with P = incident radiation power, η = fraction of power absorbed, H = thermal mass of the detector, G = thermal conductance of the link, and Θ = temperature increase above the sink temperature T.

If the radiation flux consists of a continuous background component P_0 and a sinusoidally changing signal component P_ω, one can write:

$$P = P_0 + P_\omega \exp(j\omega t) \tag{9}$$

Solving Eq. 8 for radiation described by Eq. 9 leads to:

$$\Theta_\omega = \eta P_\omega (G^2 + \omega^2 H^2)^{-\frac{1}{2}} \quad \text{and the phase angle } \rho \tag{10}$$

between P_ω and Θ_ω:

$$\rho = \tan^{-1}(\omega H/G) \tag{11}$$

For $G > \omega H$, the signal Θ_ω is frequency independent. At higher frequencies the signal will begin to roll off linearly with the inverse of ω. The characteristic response time constant τ can be defined with:

$$\tau = H/G \tag{12}$$

Typical values of τ fall between milliseconds and seconds, illustrating the slow response, which is one distinct disadvantage of thermal detectors.

After the analysis of the thermal circuit of a bolometer, we have to examine the electrical parameters. The temperature coefficient α for the resistance R_b of a bolometer is commonly defined by:

$$\alpha = \frac{1}{R_b}\left(\frac{dR_b}{dT}\right) \tag{13}$$

with R_b = resistance (Ω) and T = temperature (K). The voltage change V_s across the bolometer element can be written as:

$$V_s = I\Delta R_b = I\alpha R_b \Theta_\omega \tag{14}$$

I = current passing through the bolometer. Using the expression for Θ_ω, Eq. 10, we find:

$$V_s = \eta P_\omega (G^2 + \omega^2 H^2)^{-\frac{1}{2}} I\alpha R_b \tag{15}$$

or in the form of a responsivity R (in V/W), we find:

$$R = \eta I\alpha R_b (G^2 + \omega^2 H^2)^{-\frac{1}{2}} \tag{16}$$

Equation 16 shows that for a maximum in R, one wants to choose high values of α, R_D, I and $\eta \approx 1$. For low temperature bolometers operating at long wavelength, one cannot optimize all these parameters with a single piece of material. Recognizing this, groups at Caltech [18] and Berkeley [19] separated the functions and have built composite bolometers. These consist of an "antenna"--a thin sapphire platelet covered with 200 Å of Bi on one side, and the sensor element--a doped germanium cube acting as the thermometer [19,20]. An interesting point is the fact that the bonding material between the sapphire and the germanium piece may dominate the total heat capacity H. It turns out that epoxy resins have much higher heat capacities than pure indium solder [20]. Because the excitation currents may be many orders of magnitude higher in a bolometer than in a photoconductor, special care has to be taken in regard to the fabrication of low noise contacts. Again the metallized ion-implanted and annealed contacts have given the best results. No excess noise (1/f noise) has been observed [20] at frequencies as low as 2 Hz.

We now turn our attention to the bolometer bulk material. With the best amplifiers using cooled junction field effect transistors, one obtains the best results with bolometers and load resistors of the order of 10^6 to 10^8 Ω. The value of α should be as large as possible. We have briefly mentioned in the sections on photoconductors that a hopping conduction regime becomes significant when one goes to very low temperatures with moderately- to heavily-doped semiconductors. It is this regime which permits the fabrication of doped semiconductor bolometers of virtually any size [typical values are ~ $(0.3\ \mathrm{mm})^3$] having resistance values mentioned above. The temperature coefficient depends strongly on the degree of compensation ($N_{minority}/N_{majority}$). Because the hopping regime is based on tunneling, we can expect that small changes in the interimpurity distances (i.e. doping concentration) and the compensation will lead to large fluctuations in α and R. This has been experimentally verified and the search for suitably doped material has been purely empirical and frustrating. Changes within a slice of a given crystal were often too large to yield more than one suitable bolometer element. Impurity fluctuations have been detrimental for other semiconductor devices for totally different reasons. For example, in high voltage rectifiers and thyristors, such fluctuations lead to high electric field regions in the depletion layer under reverse bias. These high field spots reduce the maximum operating voltage and lead to large variations between otherwise identical devices.

A technique starting with the purest available material and doping it through transmutation of semiconductor host atoms has turned out to be an instantaneous success for silicon power devices [11]. Thermal neutrons from a nuclear reactor are captured by the three stable isotopes of silicon--^{28}Si, ^{29}Si, ^{30}Si. The lighter isotopes transform into the heavier stable silicon isotopes. ^{30}Si, on the other hand, becomes a ^{31}Si isotope, too rich in neutrons to remain stable. With a half life of 2.7 hrs, it decays via emission of a beta ray (electron) into a $^{31}_{15}P$ isotope. Phosphorus is a donor in Si and makes the crystals n-type. This neutron transmutation doping (NTD) technique has been rapidly implemented worldwide and approximately 100 tons of single crystal silicon per year are doped by NTD [21]. Table 1 shows the nuclear reactions taking place when germanium and gallium arsenide are transmutation doped. Those isotopes which lead to stable isotopes of the same element are not included (^{72}Ge and ^{73}Ge). Table 1 shows that in

Table 1.

Isotope Fraction	Reaction	σ_c(b)	$t_{1/2}$	Type
(20.5%)	${}^{70}_{32}Ge(n,\gamma)\ {}^{71}_{32}Ge \rightarrow {}^{71}_{32}Ga + K$	3.25	11.2d	p
(36.5%)	${}^{74}_{32}Ge(n,\gamma)\ {}^{75}_{32}Ge \rightarrow {}^{75}_{33}As + \beta^-$	0.52	82.8m	n
(7.8%)	${}^{76}_{32}Ge(n,\gamma)\ {}^{77}_{32}Ge \rightarrow {}^{77}_{33}As + \beta^- \rightarrow {}^{77}_{34}Se + \beta^-$	0.16	11.3h	n
(60.1%)	${}^{69}_{31}Ga(n,\gamma)\ {}^{70}_{31}Ga \rightarrow {}^{70}_{32}Ge + \beta^-$	1.7	21.1m	n
(39.9%)	${}^{71}_{31}Ga(n,\gamma)\ {}^{72}_{31}Ga \rightarrow {}^{72}_{32}Ge + \beta^-$	4.6	14.1h	n
(100.0%)	${}^{75}_{33}As(n,\gamma)\ {}^{76}_{33}As \rightarrow {}^{76}_{34}Se + \beta^-$	4.4	26.3h	n

the case of germanium, both acceptors and donors are produced. The ratio of donors to acceptors, i.e., the compensation K, is fixed by the isotopic abundance and the neutron capture cross sections. Because the cross sections do not exhibit precisely the same dependence on the neutron energy spectrum, one finds slight variations in the reported compensation values of K. We have adopted a value of K = 0.322 for our work [22]. The weak absorption of neutrons by Ge leads to a very uniform doping throughout large pieces of single crystal. Figure 5 shows a group of six resistivity curves (labeled with their respective Ga concentrations and NTD) as a function of the inverse absolute temperature. The abrupt change from the freeze out to the hopping regime is clearly seen in the large change of slope between 8 and 12 K. The slopes of all six curves in the hopping regime are similar. For comparison, three curves of uncompensated material are shown. We interpret the different slopes in the 1.1×10^{16} UNCOMP curve with hopping (some residual compensation is unavoidable!) between 10 and 3.5 K and with banding below 3.5 K. When the wavefunctions of the dopant atoms begin to overlap, bands of states near the corresponding band edges form and a third kind of conduction regime sets in.

Recently, a number of ultra-pure germanium crystal slices have been doped with neutron transmutation, and material suitable for bolometers operating at temperatures as low as 0.05 K is available. When plotting the logarithm of the resistivity as a function of inverse absolute temperature down to such low temperatures, one finds that the hopping regime deviates from straight lines. A better fit to straight lines is obtained by plotting the inverse of the square root of the absolute temperature on the x-axis. Certain theoretical models for hopping conduction [3] predict such a dependence. Figure 6 shows the temperature dependence of the resistivity [$\ln(\rho)$ versus $T^{-1/2}$] of six transmutation-doped germanium samples. The constants ρ_0 and Δ in the equation

$$\rho = \rho_0 \exp\left(\frac{\Delta}{T}\right)^{\frac{1}{2}} \tag{17}$$

are given in the following table.

Table 2.

total neutron dose (fluence per cm^{-2})	pre-exponential factor ρ_0 (Ω)	exponent $\Delta(K)$
7.5×10^{17}	0.375	8.96
9.25×10^{17}	0.180	8.42
1.65×10^{18}	0.174	6.27
1.88×10^{18}	0.114	5.69
3.33×10^{18}	0.149	2.50

An interesting question has recently arisen as temperatures as low as 0.1 K began to be used for bolometer operation. The low temperature heat capacity of pure insulators depends on the third power of the absolute temperature:

$$C_v = c\left(\frac{T}{\Theta}\right)^3 \tag{17}$$

with c = constant and Θ = Debye temperature of the solid. The Debye temperature of silicon Θ_{Si} = 645 K is nearly twice as high as that of germanium Θ_{Ge} = 374 K which would make Si the preferable material [23]. The fact that the impurity orbits are smaller in silicon requires larger impurity concentrations for banding conduction to occur. Whether these increased impurity concentrations over or under compensate for the advantage in Θ, has not been satisfactorily answered. It is, however, generally assumed that the Θ advantage is reduced to an unimportant magnitude and that the NTD produced Ge is preferable because of its excellent uniformity and reproducibility.

4. FURTHER DEVELOPMENTS AND CONCLUSIONS

This review of state-of-the-art photoconductors and bolometers has been aimed at materials developments and new concepts of extrinsic silicon and germanium devices. A number of exciting developments which are of great importance for certain applications can only be mentioned briefly. The field of linear and two-dimensional detector arrays is in a state of rapid development. The most recent data seem to indicate that hybrid circuits consisting of a photoconductor or photodiode array bonded with indium solder to a switched MOS readout device with up to ~ 60 x 60 elements will produce the highest performance. A very interesting feature of the newest readout devices is the option of randomly selectable readout of any given element or area of elements. This will allow the accumulation of data from areas with high information content much more rapidly than from the rest of the array.

Charge coupled devices (CCD) which have been successfully developed for visible light imaging have been adapted to a number of ways of IR imaging. Some excellent results have been achieved [24]. There exist, however, a number of basic limitations. These are due to the relatively thick absorption layers needed for IR photoconductors. The thick layers can lead to poor charge transfer efficiency. A further disadvantage of CCD devices is related to the original readout philosophy of

CCD's. They were developed for television-type imaging and are therefore dominated by the corresponding time constants. They also do not allow random readout of preferred pixels.

A third kind of array photoconductor device, the charge injection device (CID), is a monolithic combination of a standard photoconductor and a metal-insulator-semiconductor capacitor. The voltage generated across the capacitor by signal charge is regularly read out by MOS switching circuitry. CID array performance at 1 s integration time comparable to single element photoconductor performance has recently been reported [25].

A new, nonequilibrium theory of bolometer noise [26] shows that the traditionally accepted noise limits can be reduced by as much as 60% for Johnson noise and 30% for noise from phonons in the thermal link of the bolometer. Recent results with ion implanted composite bolometers corroborate the new theory [20]. Attempts to dope silicon for bolometer use with the ion implantation technique have led to encouraging results [27]. Combined with photolithographic techniques used in microelectronics, this new doping technique may make integrated bolometer arrays feasible.

In conclusion, we hope to have demonstrated that the demand for low background, NEP_{BLIP} limited infrared detectors has greatly stimulated detector materials development and detector physics. Photon noise limited detection is now possible down to a very low background flux over wavelengths ranging from 1 to 1000 μm. With this new instrumentation and additional progress to be made in the coming years, the infrared astronomy and astrophysics communities will be ready for the challenges offered by spaceborn observation platforms and telescopes.

ACKNOWLEDGMENTS

The work reported in this paper was performed in a number of laboratories by several investigators. I am indebted to P. L. Richards, U.C. Berkeley, for the use of his facilities and for many fruitful discussions and suggestions. E. Kreysa, MPI Bonn, has critically evaluated our NTD Ge and has made his data available for incorporation in this work. W. L. Hansen has strongly contributed to the growth of specially-doped germanium crystals. N. M. Haegel and M. Hueschen have characterized numerous photoconductors and have greatly advanced the understanding of the physics of these devices. The input obtained from the infrared detector users community (C. Townes, F. Low, J. Houck and many others) has been very helpful in focusing this work.

This work was supported by NASA Contract No. W-14,606 under Interagency Agreement with the Director's Office of Energy Research, Office of Health and Environmental Research, U.S. Department of Energy under Contract No. DE-AC03-76SF00098.

REFERENCES

1. See special letter section in Astrophysics J. 278, March 1, L1 ff. (1984).
2. Bratt P, "Impurity Germanium and Silicon Infrared Detectors", Chapter 2 in: Semiconductors and Semimetals, Vol. 12, Willardson R K and Beer A C, eds., Academic Press (1977). Also: "Infrared Receivers for Low Background Astronomy", NASA Technical Memorandum 78598, June 1979, available from the National Technical Information Service, Springfield, Virginia 22161, U.S.A.
3. Fritzsche H, "The Metal-Nonmetal Transition in Semiconductors", in: The Metal-Nonmetal Transition in Disordered Systems, Friedman L R and Tunstall D P, eds., Scottish Universities Summer School in Physics (1978).
4. Articles in Nuclear Radiation Detector Materials, MRS Symposia Proc. Vol. 16, Haller E E, Kraner H W and Higinbotham W A, eds., North Holland (1983).
5. Haegel N M, "Performance and Materials Aspects of Ge:Be and Ge:Ga Photoconductors for Far Infrared Detection", Thesis, University of California, Berkeley, 1983; Lawrence Berkeley Laboratory Report LBL-16694.
6. Haegel N M, Hueschen M R and Haller E E, "Development of High Responsivity Ge:Ga Photoconductors", this conference.
7. Keller W and Muehlbauer A, Floating Zone Silicon, Marcel Dekker, Inc. (1981).
8. Alexander D H, Baron R and Stafsudd O M, IEEE Trans. Electr. Dev. ED-27, No. 1, 71 (1980).
9. Frensley W R, IEEE Trans. Electr. Dev. ED-30, No. 12, 1619 (1983).
10. Baron R, Young M H, Neeland J K and Marsh O J, Appl. Phys. Lett. 30, 594 (1977).
11. Meese J M, ed., Neutron Transmutation Doping in Semiconductors, Plenum Press (1979).
12. Cross J W, Ho L T, Ramdas A K, Sauer R and Haller E E, Phys. Rev. B 28, 6953 (1983).
13. Haegel N M, Haller E E and Luke P N, Intl. J. of Infrared and Millimeter Waves 4, No. 6, 945 (1983).
14. Hall J J, Phys. Rev. 128, 68 (1961).
15. Haller E E, Hueschen M R and Richards P L, J. Appl. Phys. 34, 495 (1979).
16. Cooke R A, Nicholas R J, Stradling R A, Portal J C and Askenazy S, Solid State Comm. 26, 11 (1978).
17. Putley E H, "Thermal Detectors", in: Optical and Infrared Detectors, Keyes R J, ed., Topics in Applied Physics 19, Springer-Verlag (1980).
18. Werner M W, Elias J H, Gezari D Y, Hauser M G, and Westbrook W E, Astrophys. J. 199, L185 (1975).
19. Nishioka N S, Richards P L and Woody D P, Appl. Optics 17, 1562 (1978).
20. Lange A E, Kreysa E, McBride S E, Richards P L and Haller E E, Intl. J. Infrared and Millimeter Waves 4, No. 6, 689 (1983).
21. See review articles in Proc. 4th Intl. Neutron Transmutation Doping of Semiconductors Conference, Larabee R D, ed., Plenum Press (1984) in print.

22. Haller E E, Palaio N P, Rodder M, Hansen W L and Kreysa E, "NTD Germanium: A Novel Material for Low Temperature Bolometers", Proc. 4th Intl. Neutron Transmutation Doping of Semiconductors Conference, Larabee R D, ed., Plenum Press (1984) in print. Also: Rodder M, "Electrical Properties of Neutron-Transmutation-Doped Germanium, Thesis, University of California, Berkeley, 1982; Lawrence Berkeley Laboratory Report LBL-16216. Also: Palaio N P, Rodder M, Haller E E and Kreysa E, Intl. J. Infrared and Millimeter Waves 4, No. 6, 933 (1983).
23. See, for example, Kittel C, Introduction to Solid State Physics, 5th ed., p. 126, J. Wiley and Sons (1976).
24. See articles in "Infrared Technology Worksnop", comment eaition, McCreight C R, ed., NASA Ames Research Center, Moffett Field, CA 94035, (Fall 1983).
25. McCreight C R and Goebel J H, Appl. Optics 20, No. 18, 3189 (1981).
26. Mather J C, Appl. Optics 21, 1125 (1982).
27. Downey P M, Ph.D. Thesis, unpublished, Dept. of Physics, Massa chusetts Institute of Technology, 1980.

FIGURE CAPTIONS

Fig. 1. Schematic of a photoconductor and the associated external biasing circuit. (XBL 842-850).

Fig. 2. Hypothetical performance curve of a photoconductor. P_{CRIT} is the power below which the device is electronic noise limited and above which it is dominated by photon noise. (XBL 843-971).

Fig. 3. Photoconductive response of unstressed and uniaxially stressed Ge:Ga photoconductors (Ref. 15). (XBL 7811-6150).

Fig. 4. Basic thermal circuit of a bolometer. (XBL 826-10477).

Fig. 5. Resistivity as a function of the inverse absolute temperature for six neutron-transmutation-doped Ge samples (marked NTD) and three uncompensated Ge samples (marked UNCOMP) [21]. (XBL 823-8357).

Fig. 6. Resistivity as a function of the inverse of the square root of the absolute temperature of six transmutation-doped germanium samples. (XBL 846-2621).

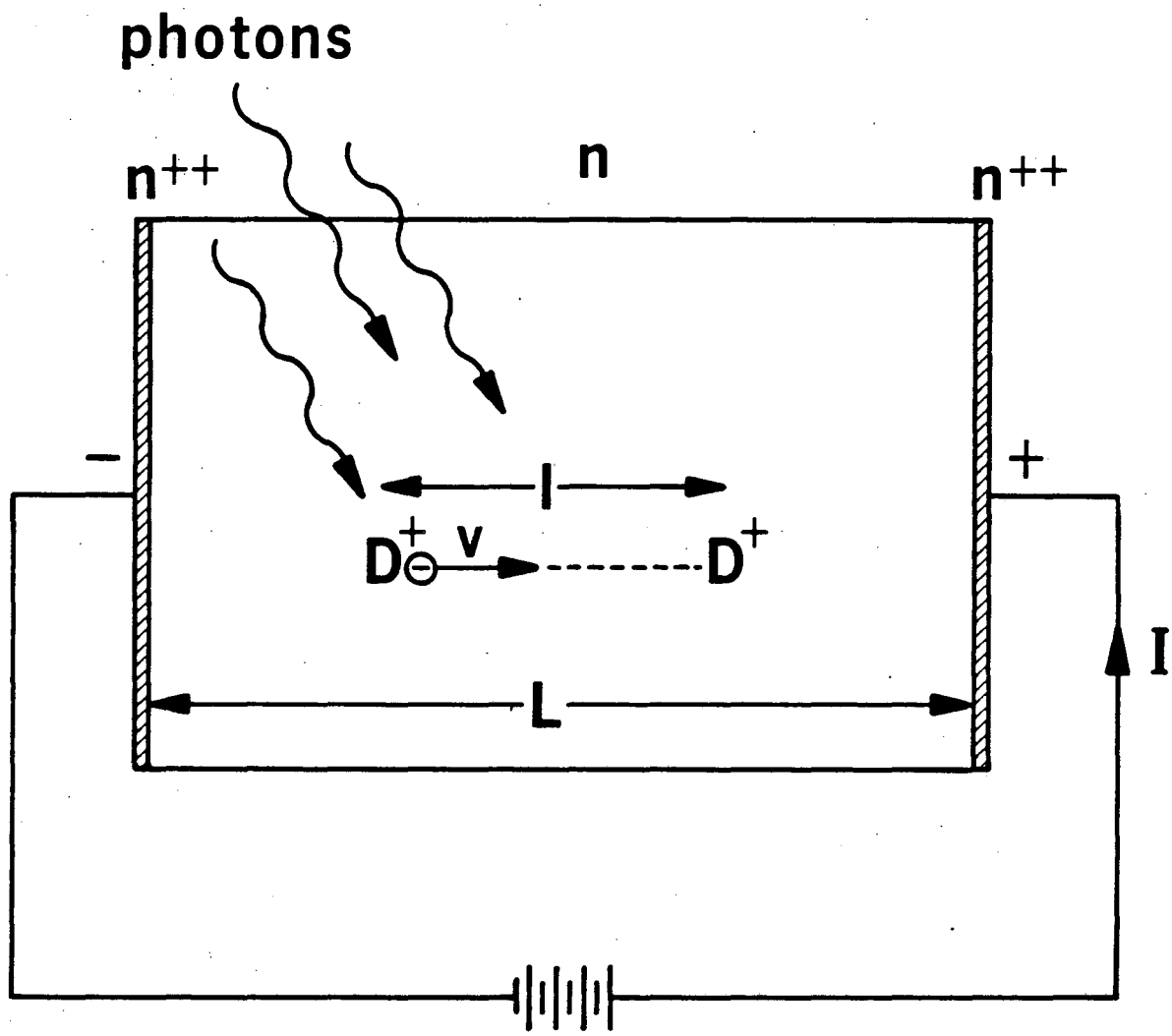

XBL 842-850

Figure 1.

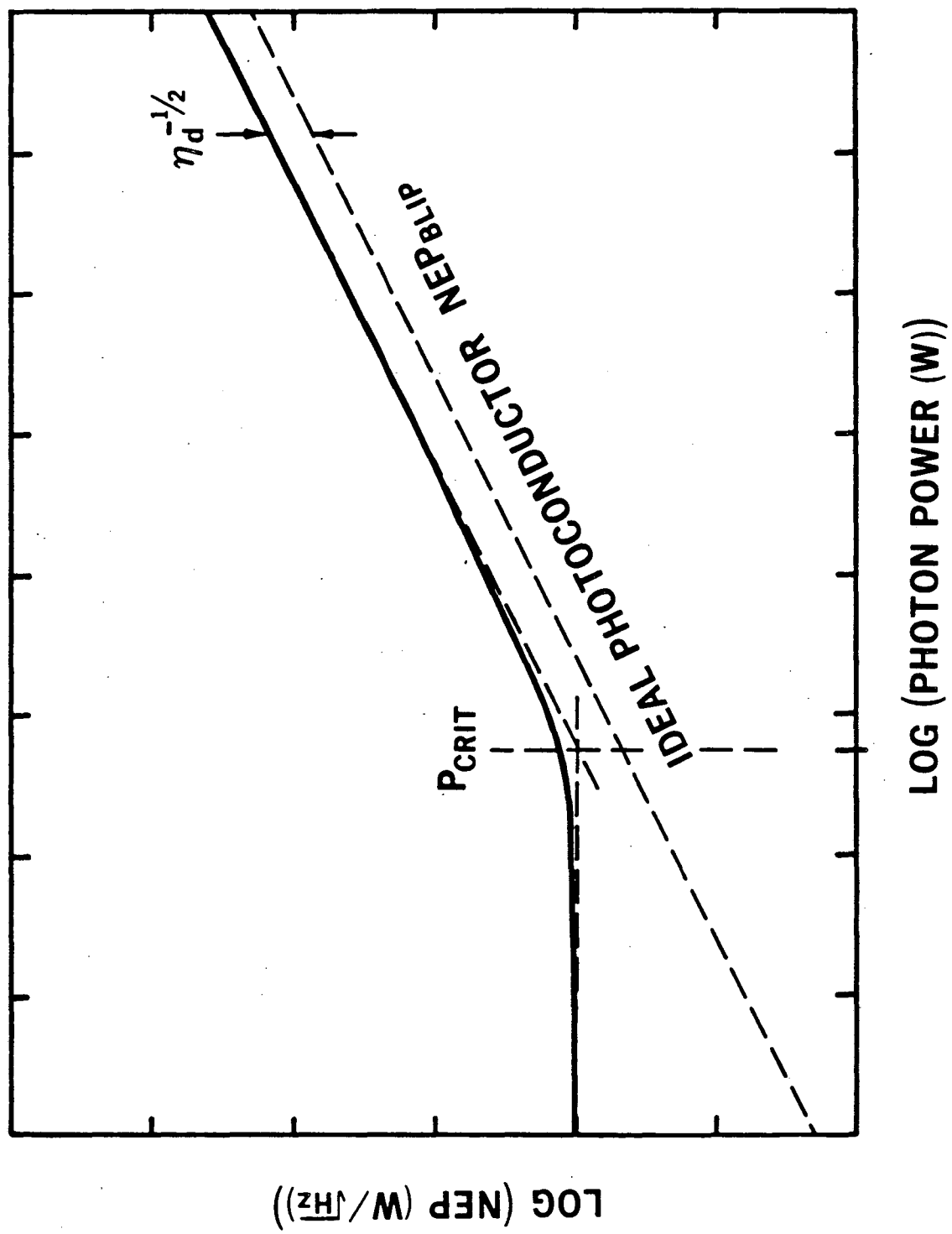

XBL 843-971

Figure 2.

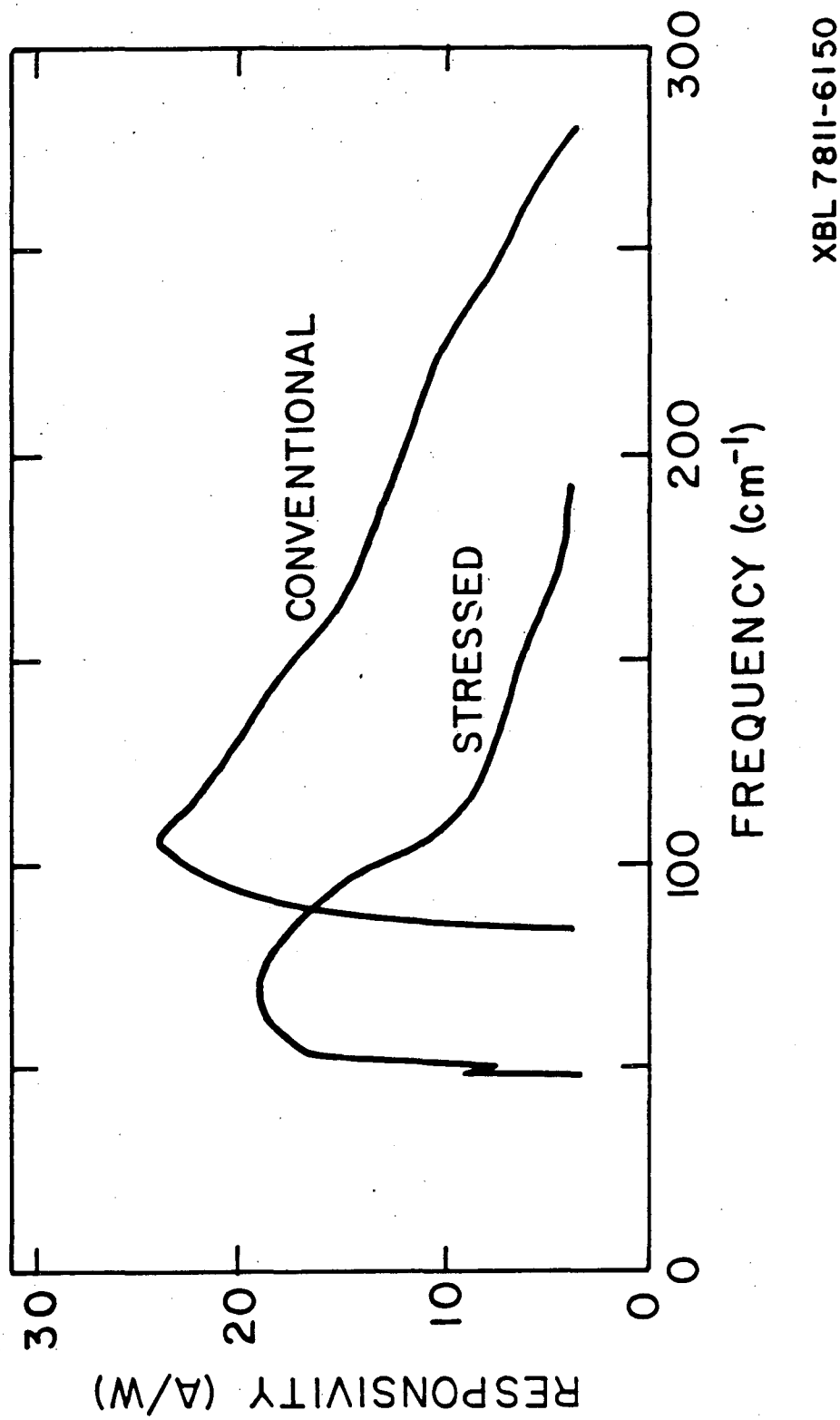
CONVENTIONAL
STRESSED
RESPONSIVITY (A/W)
30
20
10
0
0
100
200
300
FREQUENCY (cm^{-1})
XBL 7811-6150

Figure 3.

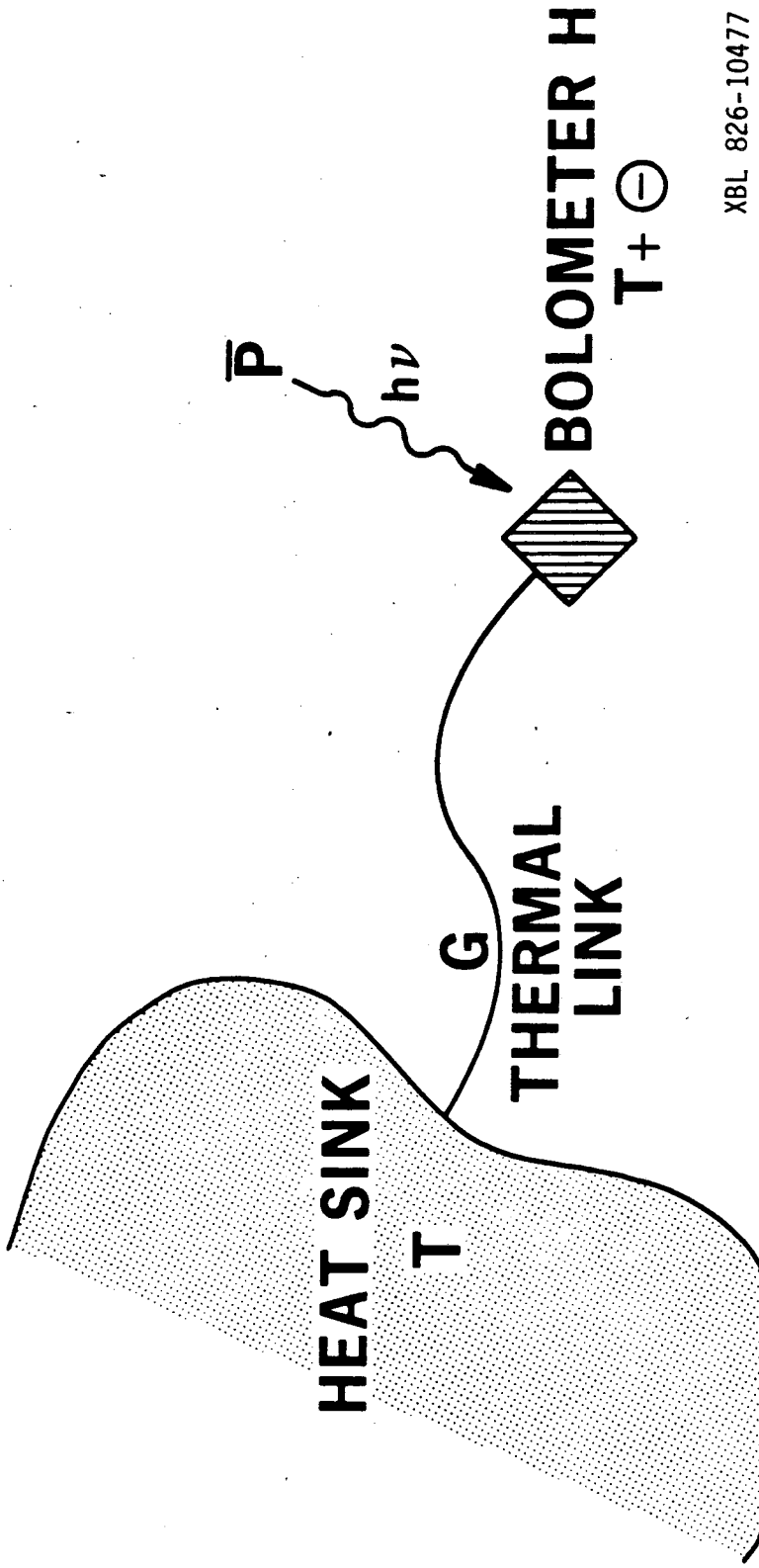
$\overline{P}$
$h\nu$
BOLOMETER H
T+ ⊖
G
THERMAL
LINK
HEAT SINK
T
XBL 826-10477

Figure 4.

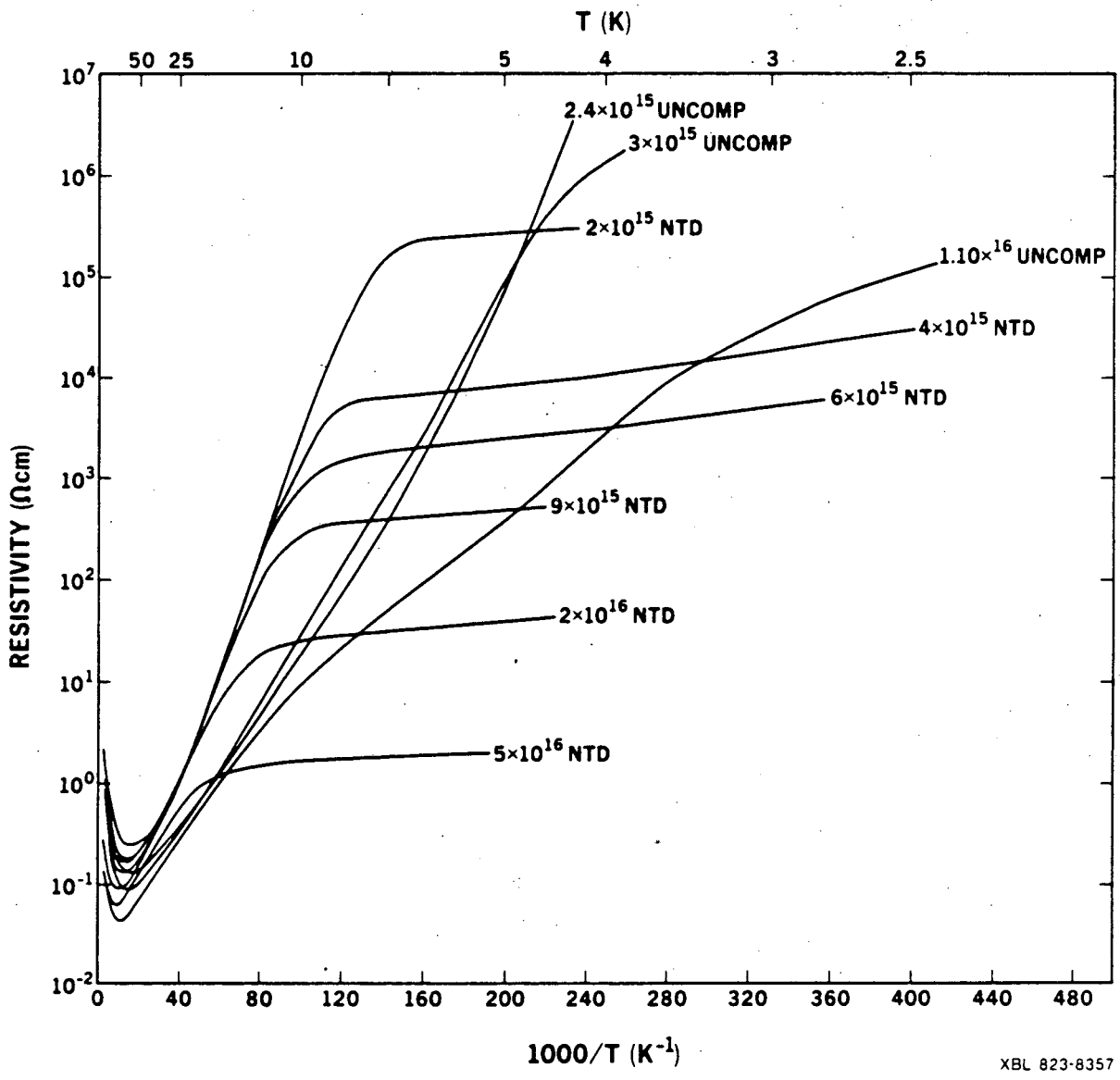
T (K)
50 25 10 5 4 3 2.5
RESISTIVITY (Ωcm)
10^7
10^6
10^5
10^4
10^3
10^2
10^1
10^0
10^{-1}
10^{-2}
2.4×10^15 UNCOMP
3×10^15 UNCOMP
2×10^15 NTD
1.10×^16 UNCOMP
4×10^15 NTD
6×10^15 NTD
9×10^15 NTD
2×10^16 NTD
5×10^16 NTD
0 40 80 120 160 200 240 280 320 360 400 440 480
1000/T (K^-1)
XBL 823-8357

Figure 5.

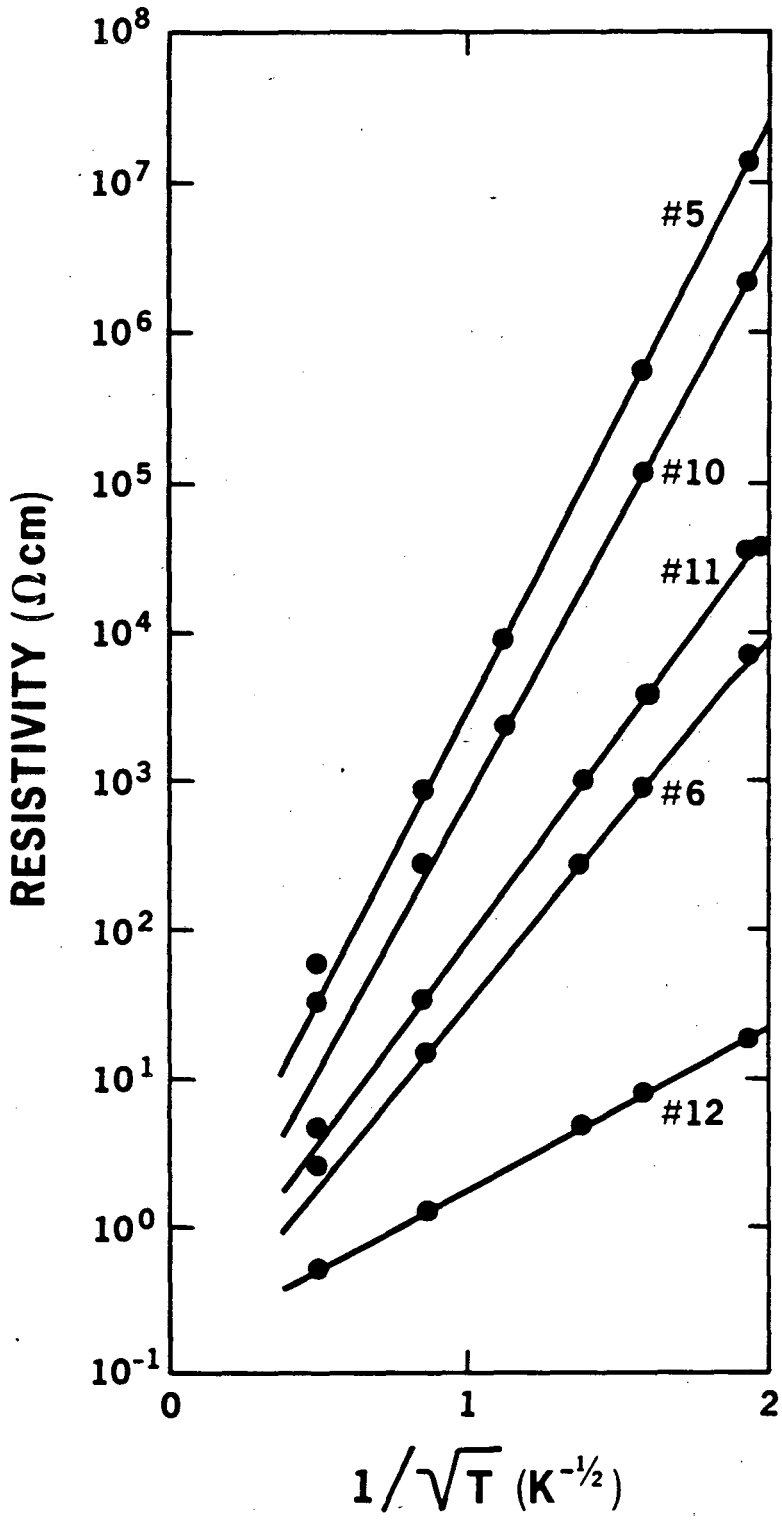

XBL 846-2621

Figure 6.

This report was done with support from the Department of Energy. Any conclusions or opinions expressed in this report represent solely those of the author(s) and not necessarily those of The Regents of the University of California, the Lawrence Berkeley Laboratory or the Department of Energy.

Reference to a company or product name does not imply approval or recommendation of the product by the University of California or the U.S. Department of Energy to the exclusion of others that may be suitable.

TECHNICAL INFORMATION DEPARTMENT
LAWRENCE BERKELEY LABORATORY
UNIVERSITY OF CALIFORNIA
BERKELEY, CALIFORNIA 94720